ChemComm

COMMUNICATION

View Article Online
View Journal | View Issue

Cite this: *Chem. Commun.*, 2025, **61**, 2325

Received 27th November 2024,
Accepted 2nd January 2025

DOI: 10.1039/d4cc06288d

rsc.li/chemcomm

Polyhydroxy starch with abundant hydroxyls and a unique structure enables uniform Zn deposition†

Ming Song,‡[a] Zhaohe Guo,‡[a] Yan Xu,*[a] Xueyao Mo,[a] Xuena Xu,[b] Limei Sun,[a] Wenyi Tan,[a] Dongliang Chao[c] and Wanhai Zhou*[c]

Zinc metal is a promising anode material for zinc-ion batteries (ZIBs), but severe side reactions and dendrite formation hinder its commercialization. In this study, starch is introduced into the $ZnSO_4$ electrolyte for stabilizing the Zn anode. With abundant hydroxyl groups, starch can reconstruct the H-bond system in the electrolyte, suppressing side reactions. Moreover, the unique ring and double-helix structures of starch show strong interactions with Zn^{2+} ions. The large molecule structure also exhibits a steric hindrance effect, regulating the diffusion and reduction of Zn^{2+}. Additionally, starch molecules can adsorb onto the Zn anode, promoting the formation of a solid–electrolyte interphase (SEI) and resulting in uniform Zn deposition along the (002) plane. Consequently, this approach enhances the stability and reversibility of the Zn anode.

The increasing importance of renewable energy sources underscores the urgent need for effective energy storage solutions.[1] Aqueous Zn-ion batteries (ZIBs) have emerged as promising candidates owing to their safety and affordability.[2,3] Zinc metal, a key component of ZIBs, boasts non-toxicity, abundant reserves, and high theoretical capacity. However, the commercial viability of ZIBs is impeded by parasitic reactions and dendrite formation.[4,5]

Various strategies have been proposed to address these issues.[6–8] Electrolyte engineering is particularly appealing due to its simplicity, cost-effectiveness, and multifunctionality.[9] Existing additives encompass a range of materials such as inorganic salts, organic solvents, and polymers.[10] Polymer additives, in particular, are characterized by multiple functional groups that can strongly interact with Zn^{2+}, thereby influencing the transfer behavior. Moreover, they have the capability to disrupt original H-bonds, which can reduce the content of active water. For example, hyaluronic acid (HA) with abundant –COOH and –OH groups, could disrupt H-bonds among water molecules, thereby inhibiting side reactions.[11] Additionally, Zn dendrite growth is believed to be influenced by the preferential growth of specific crystal planes. The preferred Zn(002) plane growth makes crystals grow at 0–30° from the Zn anode.[12] However, Zn atoms tend to deposit on the (101) plane due to their strong binding energy, leading to preferential growth of the (101) plane at an angle of 30–70° and forming Zn dendrites.[13] Introducing additives with different functional groups into the electrolyte, such as triethanolamine,[14] and *N*,*S*-CDs,[15] has been reported to induce Zn(002) plane deposition.

Starch, a low-cost natural biopolymer, has been used to prepare a gel electrolyte for zinc-air batteries due to its hydrophilicity and adhesion.[16] Here, it is introduced into the $ZnSO_4$ electrolyte for stabilizing the Zn anode. The starch (farina starch) consists of α-D-glucopyranosyl units linked *via* α-1,4-glucosidic linkages (Fig. S1, ESI†). Due to the ability of hydroxyl groups to form H-bonds, starch exhibits helical polymer chains. These chains intertwine in an anti-parallel manner, forming a characteristic double-helix structure.[17] It also can reconstruct the H-bonds in the electrolyte, suppressing water-induced reactions. Due to the intense electron density, the ring and double-helix structure with obvious steric hindrance effect has strong zincophilicity, regulating the deposition behaviour of Zn^{2+} ions. Moreover, a solid electrolyte interface (SEI) is formed. Uniform Zn deposition with exposure of the Zn(002) plane is achieved, yielding an enhanced long-term cycling stability in Zn‖Zn, Zn‖Cu and Zn‖VO_2 cells.

Generally, in a dilute electrolyte, Zn^{2+} tends to interact with surrounding electron donors, forming a $Zn[H_2O]_6^{2+}$ structure.[18] When the starch is introduced, the coordination environment of Zn^{2+} can be altered due to the dense electron density from hydroxyl groups. The interaction between Zn^{2+} and starch (including units, rings, and double helices) has been calculated using density functional theory (DFT). As illustrated in Fig. 1a, a stronger interaction is formed between Zn^{2+} and starch,

[a] *School of Materials and Chemical Engineering, Xuzhou University of Technology, Xuzhou 221018, China. E-mail: xuyan8787@163.com*
[b] *Department of Mechanical Engineering, Tsinghua University, Beijing 100084, China*
[c] *Laboratory of Advanced Materials, Aqueous Batteries Center, Shanghai Key Laboratory of Molecular Catalysis and Innovative Materials, Fudan University, Shanghai, 200433, China. E-mail: zhouwh@fudan.edu.cn*

† Electronic supplementary information (ESI) available. See DOI: https://doi.org/10.1039/d4cc06288d

‡ These authors contributed equally to this work.

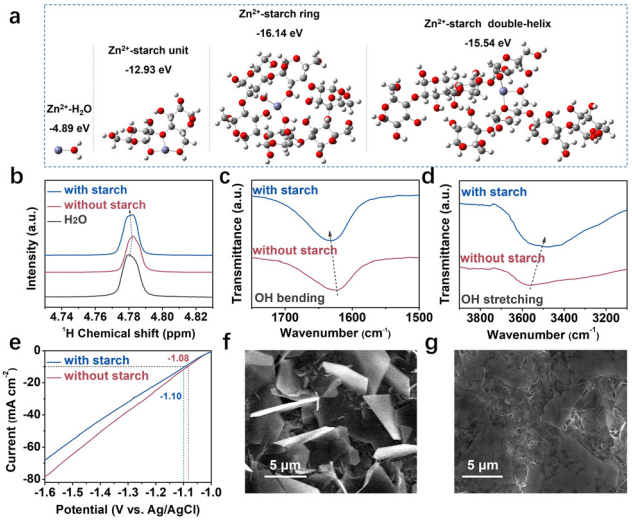

Fig. 1 (a) Binding energy of Zn^{2+} with H_2O and starch (unit, ring, and double-helix). (b) ^1H NMR spectra. FTIR spectra of OH bending (c) and stretching (d) and (e) LSV curves. SEM images of soaked Zn foil in electrolyte without (f) and with starch (g).

particularly with the ring and helix structure, which potentially alters the $Zn[H_2O]_6^{2+}$ solvation structure.

Nuclear magnetic resonance (NMR) analysis has been conducted to examine the changed solvation structure of Zn^{2+} (Fig. 1b). The ^1H peak shifts to a lower field when $ZnSO_4$ is introduced. This indicates the formation of $Zn[H_2O]_6^{2+}$, which can decrease the surrounding electron density and weaken the electrostatic shielding effect on protons.[19] Upon the introduction of starch, the ^1H peak shifted back to a higher field, indicating a changed coordination structure and formed H-bonds.[20]

The impact of starch on H-bonds has been confirmed using Fourier transform infrared spectroscopy (FTIR). A blue shift is observed in the bending vibration of H_2O (1600–1700 cm^{-1}), while the stretching vibration of H_2O (3000–3500 cm^{-1}) exhibits a notable red shift upon the introduction of starch (Fig. 1c and d). This shift indicates the formation of H-bonds between starch and water, leading to a reconstruction of the H-bond network in the electrolyte.[21] Hydrogen evolution reaction (HER) is a competitive process with the formation of H-bonds.[22] More energy may be needed to decouple the H-bonds in the reconstructed system, suppressing side reactions.

The HER and corrosion of the Zn anode in different electrolytes have been conducted using linear sweep voltammetry (LSV) and linear polarization experiments (Tafel). At 10 mA cm^{-2}, a larger overpotential (−1.10 V) is observed in the electrolyte with starch, which is 19 mV higher than that in the bare $ZnSO_4$ electrolyte. This result demonstrates the inhibitory effect of starch on H_2 generation. Additionally, a wider electrochemical window is obtained in the starch-containing electrolyte in Fig. S2 (ESI†). The Tafel plot in Fig. S3 (ESI†) indicates a lower corrosion current in the starch-containing electrolyte, suggesting the mitigation of the self-corrosion issue of the Zn anode.

The starch in inhibiting side reactions has been further investigated by immersing Zn foil in the electrolyte for 6 hours. From X-ray powder diffraction (XRD) results (Fig. S4, ESI†), $Zn_4SO_4(OH)_6{\cdot}4H_2O$ (PDF#44-0673[23]) is observed on the soaked Zn foil. Notably, the intensity is weak in the electrolyte containing starch, indicating suppressed formation of by-products. Moreover, the intensity of the Zn(002) plane is significantly enhanced in the starch-containing electrolyte compared with that in the bare $ZnSO_4$ electrolyte, with $I_{(002)}/I_{(101)}$ ratios of 3.9 and 1.8, respectively. The exposure of the Zn(002) plane facilitates horizontal Zn deposition, which is parallel to the surface of the electrode (Fig. S5, ESI†). Additionally, Zn(002) with the lowest surface energy is less reactive, contributing to the attenuation of side reactions.[24] Scanning electron microscopy (SEM) images in Fig. 1f and g show that numerous irregular flake-like Zn dendrites are present in the bare $ZnSO_4$ electrolyte, whereas the surface appears dense and flat in the starch-containing electrolyte. These SEM images corroborate the findings from the XRD analysis.

It is widely acknowledged that the morphology of initial nucleation is closely linked to the generation and growth of Zn dendrites. Uneven Zn nucleation can lead to surface protrusions on the Zn electrode, exacerbating electric field irregularities and ultimately promoting Zn dendrite formation through a "tip effect" mechanism.[25] The nucleation overpotential, which influences Zn nucleation, has been assessed by the cyclic voltammetry (CV) method. As illustrated in Fig. 2a, a higher nucleation overpotential is attained in the electrolyte containing starch, which can foster the formation of smaller Zn nuclei.[26]

The diffusion behavior of Zn^{2+} has been examined using the chronoamperometry (CA) method at −150 mV (Fig. 2b). The rapid initial increase in current density observed in both electrolytes indicates the uncontrolled 2-dimensional (2D) diffusion.[27] The continuous upward trend of current in the bare $ZnSO_4$ electrolyte suggests sustained 2D diffusion, where Zn^{2+} diffuses laterally along the Zn surface and accumulates at energetically favourable sites (protrusions, lattice defects, boundaries, impurities, *etc.*) to form initial Zn nuclei.[28] In

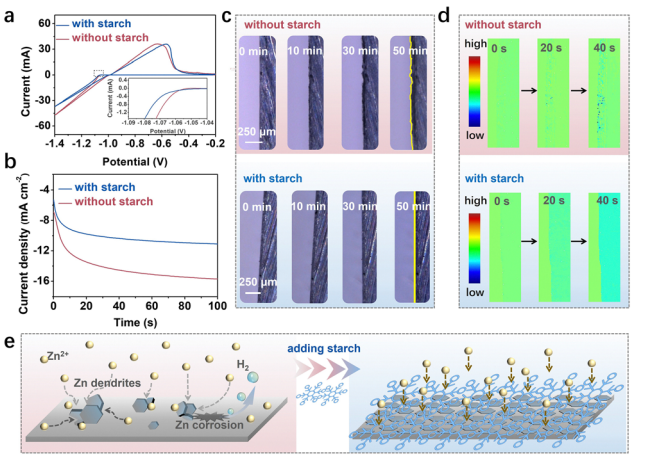

Fig. 2 (a) CV curves at a scan rate of 1 mV s^{-1}. (b) CA curves. (c) *In situ* recording images of the Zn deposition process. (d) *In situ* electrochemical digital holography for Zn^{2+} concentration evolution at the interface of the electrodes. (e) Scheme for the underlying mechanism in uniform Zn deposition.

contrast, with starch, the current stabilizes faster. The constrained 2D diffusion means that Zn^{2+} can deposit near the initial adsorption sites, resulting in more nucleation sites and uniform Zn deposition.[29]

The actual Zn deposition process has been observed using an *in situ* optical microscope. Noticeable protrusions appear in the $ZnSO_4$ electrolyte after 10 minutes, followed by uncontrolled growth of Zn dendrites (Fig. 2c). In contrast, the starch-containing electrolyte exhibits uniform and stable Zn deposition, with no apparent protrusions even after 50 minutes. The *in situ* electrochemical digital holography (EDH) technique has been employed to monitor the evolution of ion concentration during the initial Zn^{2+} reduction (Fig. 2d). The change of Zn^{2+} ion concentration can lead to a shift in colour. After 20 seconds, a local colour change is observed in both electrolytes. In the $ZnSO_4$ electrolyte, an uneven Zn^{2+} concentration is evident at the interface, which can lead to the formation of Zn dendrites. The uniform Zn^{2+} concentration in the starch-containing electrolyte indicates a uniform Zn^{2+} flux. The decreased Zn^{2+} concentration at the interface in starch-containing electrolyte should result from the adsorption of starch on the Zn anode, showing the steric hindrance effect. Due to the restrained ion and electron transfer, the Zn deposition process can be modulated. This speculation is verified by the electrochemical impedance spectroscopy (EIS) and the contact angle tests. The EIS results in Fig. S6 (ESI†) confirm the restrained reduction of Zn^{2+} ions. The lower contact angle between the Zn anode and the electrolyte containing starch in Fig. S7 (ESI†) indicates the higher surface energy at the interface between the Zn anode and electrolyte with starch, indicating the adsorption of starch molecules on the Zn anode.[30]

Based on the above analysis, it can be speculated that the starch molecule can reconstruct the H-bond system, suppressing side reactions. Moreover, it can interact with Zn^{2+} and adsorb on the electrode, directing the Zn^{2+} diffusion and reduction (Fig. 2e).

The stability of the Zn anode has been investigated using Zn‖Zn symmetric cells. As presented in Fig. 3a and Fig. S8 (ESI†), the cells in the $ZnSO_4$ electrolyte can only work steadily for about 200 h (5 mA cm^{-2} and 1 mA h cm^{-2}), 50 h (5 mA cm^{-2} and 5 mA h cm^{-2}), and 110 h (10 mA cm^{-2} and 5 mA h cm^{-2}) under various conditions. When the starch is introduced, there is an apparent improvement. The cycling life of Zn‖Zn cells increased to 1500 h, 225 h, and 350 h. The Zn‖Zn cells in the electrolyte with 0.1 and 0.4 mg mL^{-1} starch also exhibit an improved performance (Fig. S9 and S10, ESI†) compared to the bare $ZnSO_4$ electrolyte. As starch has a steric hindrance effect, 0.2 mg mL^{-1} is the optimum concentration. It shows a comparable performance with the reported results (Table S1, ESI†). Besides, the better rate performance and cycling stability at 30 mA cm^{-2} of Zn‖Zn cells in electrolyte with additive corroborate the effectiveness of starch (Fig. S11 and S12, ESI†). The coulombic efficiency (CE) has been confirmed by the Zn‖Cu cells. As shown in Fig. 3b and Fig. S13 (ESI†), a more stable CE is achieved in the electrolyte with starch. The average CE is 99% under the condition of 1 mA cm^{-2} and 0.5 mA h cm^{-2} for 1750 cycles. In sharp contrast, in the $ZnSO_4$ electrolyte, there are fluctuant voltage profiles with a low CE of 97% for about 210 cycles. The Zn deposition behaviour (plating and stripping) on Cu foil at 20 mA cm^{-2} has been studied. As shown in Fig. S14 (ESI†), there are flat Zn deposits on Cu foil in the electrolyte with starch.

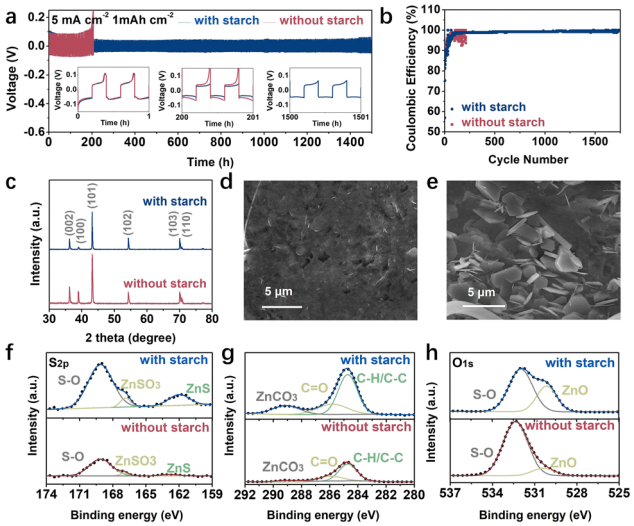

Fig. 3 (a) Cycling performance of Zn‖Zn cells at 5 mA cm^{-2} and 1 mA h cm^{-2}. (b) CE of Zn‖Cu cells at 1 mA cm^{-2} and 0.5 mA h cm^{-2}. (c) XRD profile of cycled Zn anodes; SEM images of cycled Zn anodes in the electrolyte (d) with and (e) without starch. XPS spectrum of S 2p (f), C 1s (g) and O 1s (h) of the cycled Zn anodes.

The morphology and structure of the cycled Zn electrolyte after 50 cycles have also been analyzed. The XRD results in Fig. 3c exhibit a higher $I_{(002)}/I_{(101)}$ ratio of 3.87 for the electrolyte with starch, while it is 1.50 in the $ZnSO_4$ electrolyte, indicating a preferential exposure of the (002) plane. Compared to Fig. 3d and e, the compact, flat, and smooth Zn anode is achieved in electrolyte with starch, consistent with the XRD results.

The surface chemistry of the cycled Zn anode has been investigated by X-ray photoelectron spectroscopy (XPS) after Ar^+ sputtering (5 nm). The S 2p spectra indicate the presence of S–O, $ZnSO_3$, and ZnS components, with the S–O component from SO_4^{2-} being the main component.[31] The prominent ZnS peak in the electrolyte with starch indicates the formation of solid electrolyte interphase (SEI). In the C 1s spectra, C–C/C–H, C–O, and $ZnCO_3$ can be observed,[32] derived from CO_2 and starch. The much higher intensity in the electrolyte with starch confirms the contribution of partial decomposition of starch. Additionally, as further confirmed by O 1s spectra, more ZnO is formed in the electrolyte with starch.[33] Therefore, it can be speculated that the SEI layer consisting of $ZnCO_3$, ZnS, and ZnO is formed on the Zn surface in the electrolyte with starch. The XPS spectrum of Zn 2p in Fig. S15 (ESI†) also affirms the influence of starch on the surface chemistry of the Zn electrode.

The inclusion of starch in the electrolyte is demonstrated to enhance the performance of Zn‖VO_2 full cells, highlighting the significant potential for practical ZIBs. The synthesized VO_2 is confirmed *via* XRD (JCPDF# 31-1438), as depicted in Fig. S16 (ESI†). The SEM result in Fig. S17 (ESI†) reveals its rod-like morphology. The rate capability of Zn‖VO_2 cells in both electrolytes is depicted in

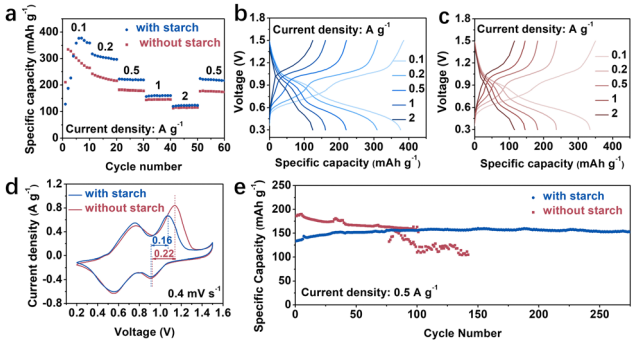

Fig. 4 (a) Rate performance. GCD curves in electrolyte (b) with and (c) without starch. (d) CV curves. (e) Long-term stability of the Zn||VO_2 cell.

Fig. 4a–c at 0.1–2 A g^{-1}. Remarkably, the cells utilizing the electrolyte with starch exhibit a higher capacity compared to those using the bare $ZnSO_4$ electrolyte. The cyclic voltammetry (CV) curves presented in Fig. 4d exhibit similar profiles in both electrolytes, confirming an unaffected charge storage mechanism. Noteworthy is the lower voltage polarization (0.16 V) observed in the electrolyte with starch compared to the bare $ZnSO_4$ electrolyte (0.22 V). The long-term cycling performance shown in Fig. 4e demonstrates the full cells in the starch-containing electrolyte maintaining a more stable performance, retaining a capacity of 155 mA h g^{-1} after 250 cycles at 0.5 A g^{-1}. Interestingly, the battery capacity in the bare $ZnSO_4$ electrolyte is higher during the initial 10 cycles, possibly attributed to proton embedding, by-product contributions to capacity, and the rapid charge transfer facilitated by the Zn anode's rough surface.

In summary, starch is introduced into the $ZnSO_4$ electrolyte. Due to the hydroxyl groups, the original H-bond system is altered, inhibiting the water-triggered reactions. Moreover, the large molecule structure enables starch with a steric hindrance effect, and the ring and helix structure has a stronger interaction with Zn^{2+}, which can modulate the diffusion and reduction of Zn^{2+}. In addition, SEI is formed on the Zn surface in the electrolyte with starch, facilitating the Zn deposition along with the (002) plane. Consequently, highly stable Zn||Zn, Zn||Cu, and Zn||VO_2 cells are achieved. This study offers a cost-effective and environmentally friendly electrolyte additive for stabilizing Zn anodes, thus advancing the development of ZIBs. The long-term stability of starch, as well as its stability under extreme conditions, should be studied in the future.

This work was financially supported by the National Natural Science Foundation of China (No. 22279023, 22075115, and 22309031), the Natural Science Foundation of the Jiangsu Higher Education Institutions of China (No. 23KJB480009), the Xuzhou Science and Technology Project (No. KC23033), and the Shanghai Science and Technology Innovation Action Plan Morning Star Project (Sail Special) (No. 23YF1401800).

Data availability

The data supporting this article have been included as part of the ESI.†

Conflicts of interest

There are no conflicts to declare.

References

1 A. Yu, W. Zhang, N. Joshi and Y. Yang, *Energy Storage Mater.*, 2024, **64**, 103075.
2 M. Al-Abbasi, Y. Zhao, H. He, H. Liu, H. Xia, T. Zhu, K. Wang, Z. Xu, H. Wang, W. Zhang, Y. Lai and M. Ge, *Carbon Neutralization*, 2024, **3**, 108–141.
3 W. Zhang, Y. Chen, H. Gao, W. Xie, P. Gao, C. Zheng and P. Xiao, *Mater. Futures*, 2023, **2**, 042102.
4 J. Yang, R. Zhao, Y. Wang, Z. Hu, Y. Wang, A. Zhang, C. Wu and Y. Bai, *Adv. Funct. Mater.*, 2023, **33**, 2213510.
5 Y. Zuo, K. Wang, P. Pei, M. Wei, X. Liu, Y. Xiao and P. Zhang, *Mater. Today Energy*, 2021, **20**, 100692.
6 G. Li, L. Sun, S. Zhang, C. Zhang, H. Jin, K. Davey, G. Liang, S. Liu, J. Mao and Z. Guo, *Adv. Funct. Mater.*, 2023, **34**, 2301291.
7 X. He, M. Kwon, J. Chung, K. Lee, Y. Choi, Y. Im, J. Jang, Y. Choi and H. J. Yoon, *Small*, 2024, **20**, 2403537.
8 H. Li, Z. Liu, Y. Tang, S. Liang and G. Fang, *cMat*, 2024, **1**, e25.
9 H. Li, S. Guo and H. Zhou, *Energy Storage Mater.*, 2023, **56**, 227–257.
10 Y. Li, H. Yao, X. Liu, X. Yang and D. Yuan, *Nano Res.*, 2023, **16**, 9179–9194.
11 B. Wang, R. Zheng, W. Yang, X. Han, C. Hou, Q. Zhang, Y. Li, K. Li and H. Wang, *Adv. Funct. Mater.*, 2022, **32**, 2112693.
12 X. Liang, X. Chen, Z. Zhai, R. Huang, T. Yu and S. Yin, *Chem. Eng. J.*, 2024, **480**, 148040.
13 H. Zhang, Y. Zhong, J. Li, Y. Liao, J. Zeng, Y. Shen, L. Yuan, Z. Li and Y. Huang, *Adv. Energy Mater.*, 2022, **13**, 2203254.
14 W. Ge, H. Peng, J. Dong, G. Wang, L. Cui, W. Sun, X. Ma and J. Yang, *Chem. Commun.*, 2024, **60**, 750–753.
15 Z. Xu, H. Li, Y. Liu, K. Wang, H. Wang, M. Ge, J. Xie, J. Li, Z. Wen, H. Pan, S. Qu, J. Liu, Y. Zhang, Y. Tang and S. Chen, *Mater. Horiz.*, 2023, **10**, 3680–3693.
16 Y. Zuo, K. Wang, M. Wei, S. Zhao, P. Zhang and P. Pei, *Cell Rep. Phys. Sci.*, 2022, **3**, 100687.
17 S. J. Zhang, J. Hao, H. Li, P. F. Zhang, Z. W. Yin, Y. Y. Li, B. Zhang, Z. Lin and S. Z. Qiao, *Adv. Mater.*, 2022, **34**, 2201716.
18 J. Cao, D. Zhang, X. Zhang, Z. Zeng, J. Qin and Y. Huang, *Energy Environ. Sci.*, 2022, **15**, 499–528.
19 Z. Hu, F. Zhang, A. Zhou, X. Hu, Q. Yan, Y. Liu, F. Arshad, Z. Li, R. Chen, F. Wu and L. Li, *Nano-Micro Lett.*, 2023, **15**, 171.
20 H. Wang, W. Ye, B. Yin, K. Wang, M. S. Riaz, B. B. Xie, Y. Zhong and Y. Hu, *Angew. Chem., Int. Ed.*, 2023, **62**, e202218872.
21 K. Bao, M. Wang, Y. Zheng, P. Wang, L. Yang, Y. Jin, H. Wu and B. Sun, *Nano Energy*, 2024, **120**, 109089.
22 T. Wang, Z. Tian, Z. You, Z. Li, H. Cheng, W. Li, Y. Yang, Y. Zhou, Q. Zhong and Y. Lai, *Energy Storage Mater.*, 2022, **45**, 24–32.
23 P. Wang, X. Xie, Z. Xing, X. Chen, G. Fang, B. Lu, J. Zhou, S. Liang and H. J. Fan, *Adv. Energy Mater.*, 2021, **11**, 2101158.
24 M. Zhou, S. Guo, J. Li, X. Luo, Z. Liu, T. Zhang, X. Cao, M. Long, B. Lu, A. Pan, G. Fang, J. Zhou and S. Liang, *Adv. Mater.*, 2021, **33**, 2100187.
25 Y. Zhang, X. Fu, Y. Ding, Y. Liu, Y. Zhao and S. Jiao, *Small*, 2024, **20**, 2311407.
26 C. Meng, W. He, L. Jiang, Y. Huang, J. Zhang, H. Liu and J. J. Wang, *Adv. Funct. Mater.*, 2022, **32**, 2207732.
27 Y. Liang, M. Qiu, P. Sun and W. Mai, *Chem. Sci.*, 2024, **15**, 1488.
28 C. Nie, G. Wang, D. Wang, M. Wang, X. Gao, Z. Bai, N. Wang, J. Yang, Z. Xing and S. Dou, *Adv. Energy Mater.*, 2023, **13**, 2300606.
29 L. Zhang, L. Miao, W. Xin, H. Peng, Z. Yan and Z. Zhu, *Energy Storage Mater.*, 2022, **44**, 408–415.
30 X. Shi, J. Wang, F. Yang, X. Liu, Y. Yu and X. Lu, *Adv. Funct. Mater.*, 2022, **33**, 2211917.
31 L. Cao, D. Li, E. Hu, J. Xu, T. Deng, L. Ma, Y. Wang, X.-Q. Yang and C. Wang, *J. Am. Chem. Soc.*, 2020, **142**, 21404–21409.
32 C. Meng, W. He, H. Tan, X. Wu, H. Liu and J. Wang, *Energy Environ. Sci.*, 2023, **16**, 3587–3599.
33 H. Dou, X. Wu, M. Xu, R. Feng, Q. Ma, D. Luo, K. Zong, X. Wang and Z. Chen, *Angew. Chem., Int. Ed.*, 2024, **63**, e202401974.

